Even-odd effect for spin current through a thin antiferromagnetic insulator

Niklas Rohling [1] and Roberto E. Troncoso[2,3]

[1]*Department of Physics, University of Konstanz, D-78457 Konstanz, Germany*

[2]*Center for Quantum Spintronics, Department of Physics, Norwegian University of Science and Technology, NO-7491 Trondheim, Norway*

[3]*School of Engineering and Sciences, Universidad Adolfo Ibáñez, Av. Diag. Las Torres 2640, 7941169 Santiago, Chile*

(Received 19 April 2023; revised 15 September 2023; accepted 17 October 2023; published 15 December 2023)

Magnon spin transport in a metal–antiferromagnetic insulator–ferromagnetic insulator heterostructure is considered. The spin current is generated via the spin Seebeck effect and in the limit of the clean sample where the effects of interface imperfections and lattice defects are excluded. For NiO as an antiferromagnetic insulator we have a magnetic order of antiferromagnetically combined planes which are internally in ferromagnetic order. We find that the sign of the spin current depends on the magnetization direction of the plane next to the metal resulting in an even-odd effect for the spin current. Moreover, as long as damping is excluded, this even-odd effect is the only remaining dependence on the NiO thickness for high temperatures.

DOI: 10.1103/PhysRevB.108.214416

I. INTRODUCTION

Leveraging spin angular momentum in magnetic insulators gathers considerable interest due to intrinsic low-dissipative transport properties. Spin transport experiments on heavy metal–ferromagnet (HM-FM) heterostructures have shown an enhancement when a thin NiO antiferromagnetic (AFM) layer is placed in between, forming, e.g., a platinum–NiO–yttrium iron garnet (YIG) trilayer [1–3] (see Fig. 1). Such an enhancement is described by theoretical models both in the diffusive limit [4] and when transport is governed by evanescent spin waves in the NiO layer [5]. However, various issues are far from being understood, such as the relation between the crystal and the magnetic configurations of the AFM, as well as interfacial properties at each contact. Note that there was a significant sample dependence in the experiments which might be due to the properties just mentioned varying from sample to sample. Further experimental investigations related to spin transport through NiO layers include the study of spin Hall magnetoresistance in ferromagnetic insulator–NiO–heavy metal systems [6–8], spin transport from a ferromagnetic to a nonmagnetic metal [9] and from one magnetic metal to another [10], as well as nonlocal spin transport in a Pt-NiO-YIG trilayer [11].

The spin current in Refs. [1,2] were generated via ferromagnetic resonance by a microwave field. Using a thermal gradient to produces spin currents via the spin Seebeck effect instead, as demonstrated in Ref. [3], allows further insights as more magnon modes are involved in the transport of spin. Further, spin-Seebeck-effect transport experiments have been performed with NiO [12] and a metallic AFM in between the HM-FM structure [13]. In contrast to Ref. [3], Refs. [12,13] report the absence of enhancement of spin currents compare to the HM-FM bilayer for most of the parameters. What was found in all three works [3,12,13] was a thickness dependence of the peak temperature, which is the temperature allowing the strongest spin transport. The peak temperature was found to be increasing with the thickness of the antiferromagnetic layers. In contrast, in Ref. [14] studying epitaxial NiO in the [001] direction, no peak temperature was found up to room temperature, which is attributed to a higher Néel temperature for epitaxial NiO. Furthermore, Ref. [14] reports no spin transport enhancement by the NiO layer for YIG-NiO-Pt, but for Fe_3O_4-NiO-Pt trilayers.

In this paper, we investigate how the AFM layers oriented in the (111) direction—namely the number of atomic planes in the transport direction—impact the spin current propagation. We focus on the spin Seebeck effect across a clean and ideal interface. We find that the sign of the spin current is determined by the number of atomic NiO planes being even or odd. Additionally, we find that in the limit of high temperatures, this even-odd effect is the only remaining dependence on the NiO thickness in the clean limit considered here. This is due to the normalization condition for magnons as bosonic modes.

II. MODEL

We consider a trilayer system with the antiferromagnetic layers (NiO) in between, with the x axis parallel to the (111) direction, orthogonal to the interface, and the hard in-plane axis along y [15]. The spin Hamiltonian of the system is

$$H_{\mathrm{AFM}} = \frac{1}{2}\sum_{\mathbf{r}\in\mathrm{AFM}}\Bigg[J_1\sum_{\boldsymbol{\delta}}\mathbf{S}_{\mathbf{r}}\cdot\mathbf{S}_{\mathbf{r}+\boldsymbol{\delta}} + J_2\sum_{\boldsymbol{\eta}}\mathbf{S}_{\mathbf{r}}\cdot\mathbf{S}_{\mathbf{r}+\boldsymbol{\eta}} + 2D_1\left(S^x_{\mathbf{r}}\right)^2 + 2D_2\left(S^y_{\mathbf{r}}\right)^2\Bigg], \tag{1}$$

where the exchange interactions $J_1 < 0$ and $J_2 > 0$ are the exchange couplings to the nearest and next-nearest neighbors, respectively. The biaxial magnetocrystalline anisotropy is parametrized by the strengths D_1 and D_2 and the vectors joining nearest and next-nearest neighbors are $\boldsymbol{\delta}$ and $\boldsymbol{\eta}$, respectively. The magnetic parameters we use are $J_1 = -16$ K, $J_2 = 221$ K, $D_1 = 1.13$ K, and $D_2 = 0.06$ K [16]. The anisotropies D_1 and D_2 complicate the considerations as the quantization

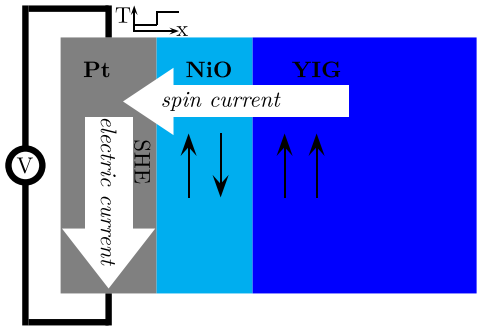

FIG. 1. Schematic setup consisting of a NM-AFM-FM trilayer heterostructure. As a model system it is considered a platinum (Pt), a thin antiferromagnetic NiO layer, and yttrium iron garnet (YIG) film, which is in good approximation a ferromagnet. A thermal gradient yields spin transport through the metal-insulator interface, which causes an electric current in Pt due to the inverse spin Hall effect (SHE) which allows detection of the spin current by electrical means.

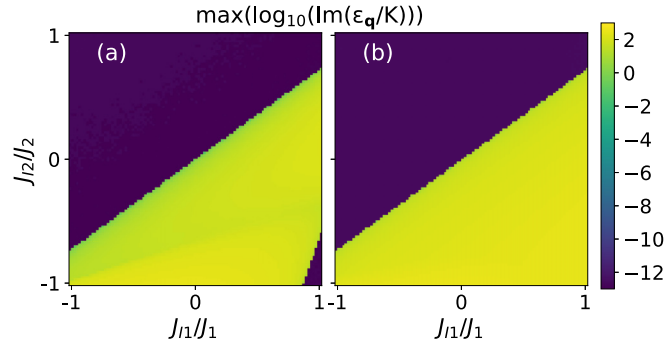

FIG. 2. Stability of the magnetic configuration where the spins of the NiO layer neighboring the FMI are pointing in the $-z$ direction while the FMI is magnetized in the $+z$ direction: For this magnetic configuration we perform a Holstein-Primakoff transformation, truncate at second order in the creation/annihilation operators, and compute the eigenvalues $\varepsilon_{\mathbf{q}}$ of the dynamical matrix (see the Appendix for details). An imaginary component above numerically uncertainties, around 10^{-12} K, is an indication for the presumed magnetic configuration to be unstable. We plot the maximum value of the decadic logarithm of the imaginary part of the resulting eigenvalues (in units of degrees Kelvin). (a) A single atomic NiO layer and five FMI layers. (b) Four NiO layers and five FMI layers.

axes of the magnons get tilted. However, in this case, they are negligibly small, so we will set in the following $D_1 = D_2 = 0$, the case of finite D_1 and D_2 is discussed in the Appendix. The spin system in the ferromagnetic insulator (FMI) shares the same fcc lattice as the AFM to avoid the influence of interface roughness and lattice mismatch. Thus the Hamiltonian is

$$H_{\mathrm{FMI}} = \frac{1}{2}\sum_{\mathbf{r}\in \mathrm{FI}}\left[J_F \sum_{\delta} \mathbf{S}_{\mathbf{r}}\cdot\mathbf{S}_{\mathbf{r}+\delta} - 2K_F\left(S^z_{\mathbf{r}}\right)^2\right], \qquad (2)$$

with J_F the exchange coupling and K_F the uniaxial easy-axis anisotropy. The parameters are chosen such that the saturation magnetization and low-energy dispersion of YIG is matched, with a (nonphysical) spin quantum number of $S_F = 0.16$ and $J_F = -400$ K, as well as a small anisotropy $K_F = 10^{-5}|J_F|$. The AFM-FMI interaction is

$$H_{\text{AFM-FMI}} = J_{I1}\sum_{\substack{\mathbf{r}\in\mathrm{AFM}\\ \mathbf{r}+\delta\in\mathrm{FMI}}} \mathbf{S}_{\mathbf{r}}\cdot\mathbf{S}_{\mathbf{r}+\delta} + J_{I2}\sum_{\substack{\mathbf{r}\in\mathrm{AFM}\\ \mathbf{r}+\eta\in\mathrm{FMI}}} \mathbf{S}_{\mathbf{r}}\cdot\mathbf{S}_{\mathbf{r}+\eta}, \quad (3)$$

with $J_{I1,I2}$ the interfacial antiferromagnetic exchange coupling. The metal is described by a simple tight-binding model, $H_M = -t\sum_{\sigma=\uparrow,\downarrow}\sum_{\mathbf{r},\delta}(c^\dagger_{\mathbf{r}\sigma}c_{\mathbf{r}+\delta,\sigma} + \mathrm{H.c.})/2$, where $\boldsymbol{\delta}$ is again the vector to a nearest neighbor and the hopping energy is assumed to be $t = 1$ eV $= 1.16\times10^4$ K.

III. MAGNETIC STABILITY AND DYNAMICS

We now investigate the stability of the magnetic configuration of the joint NiO-ferromagnet system. We consider the AFM and the FMI as a joint system, $H_I = H_{\mathrm{AFM}} + H_{\mathrm{FMI}} + H_{\text{AFM-FMI}}$, and determine the classical ground state, shown at Fig. 2, where the spins point in the $+z$ or $-z$ direction, while the configuration with spins pointing out of the interface plane are energetically not desired. Note that we have a different number of layers with B ($-z$ spin direction) and A ($+z$ spin direction) configurations as the spins in the FMI all belong to the A configuration. Note further that in contrast to the typical situation of an antiferromagnet, our system is also not invariant under interchanging the A and the B sublattices within the NiO layer (even if the number of layers in the x direction is even) because of the coupling to the FMI.

Later, we study the low-energy spin dynamics around the classical ground state. We perform a Holstein-Primakoff transformation [17] around the classical ground state and truncate after second order in the creation and annihilation operators. Then, we continue with a Fourier transform in the yz plane. Finally a multiflavor Bogoliubov transformation (see, e.g., Ref. [18]) yields the magnonic eigenstates of the system. We solve the remaining eigenvalue problem for any in-plane magnon momentum, $\mathbf{q}_\parallel = q_y\mathbf{e}_y + q_z\mathbf{e}_z$, numerically and label the eigenstates formally by q_x. This also allows to investigate the stability of the initially guessed ground state, as imaginary components in the eigenenergy indicate that this state was unstable (see the Appendix for details).

IV. SPIN SEEBECK EFFECT

The spin Seebeck effect is the generation of a spin current due to a thermal gradient. This can originate in the magnon's response to a thermal gradient and in spin-phonon drag (see Ref. [19] for an overview). Here, we focus on a temperature difference at the metal-insulator interface and disregard the influence by phonons. We compute the magnon spin current based on the Fermi's golden rule formalism [20,21]. The transition from an initial (i) and final (f) magnonic state is given by $I_{i\to f} = 2\pi|\langle\psi_f|H_{\mathrm{Int}}|\psi_i\rangle|^2\delta(E_f - E_i)/\hbar$, where the interface exchange interaction between the metal and the AFM is $H_{\mathrm{Int}} = J_I\sum_{\mathbf{r}\in M,\mathbf{r}+\delta\in\mathrm{AFM}}\sum_{\sigma,\sigma'=\uparrow,\downarrow} c^\dagger_{\mathbf{r}\sigma}\boldsymbol{\sigma}_{\sigma\sigma'}c_{\mathbf{r}\sigma'}\cdot\mathbf{S}_{\mathbf{r}+\delta}$, where J_I is the interfacial nearest-neighbor exchange coupling between the metal and the AFM and $\boldsymbol{\sigma}$ is a vector of Pauli matrices. We can write the interaction Hamiltonian in terms

of the magnonic eigenmodes of the insulator,

$$H_{\rm Int} = \sum_{\mathbf{k}\mathbf{k}'\mathbf{q}} \left[V^{\alpha}_{\mathbf{q}\mathbf{k}\mathbf{k}'} \alpha_{\mathbf{q}} c^{\dagger}_{\downarrow\mathbf{k}} c_{\uparrow\mathbf{k}'} + V^{\beta}_{\mathbf{q}\mathbf{k}\mathbf{k}'} \beta^{\dagger}_{-\mathbf{q}} c^{\dagger}_{\uparrow\mathbf{k}} c_{\downarrow\mathbf{k}'} \right] + \text{H.c.},$$

where $V^{\alpha,\beta}_{\mathbf{q}\mathbf{k}\mathbf{k}'}$ represents the electron-magnon scattering amplitudes for each magnon mode. For the current from the α magnons, we obtain—under the assumption that the electrons are in thermal equilibrium and that only electrons with energies close to the Fermi energy E_F can contribute significantly—the general expression

$$I^{\alpha} = \frac{2\pi}{\hbar} \sum_{\mathbf{k}\mathbf{k}'\mathbf{q}} \int d\varepsilon\, (\varepsilon + \Delta\mu) \left[n_B\left(\frac{\varepsilon + \Delta\mu}{k_B T_e}\right) - n_I(\varepsilon) \right] \times \left| V^{\alpha}_{\mathbf{q}\mathbf{k}\mathbf{k}'} \right|^2 \delta(E_F - E_{\mathbf{k}}) \delta\left(\varepsilon - \varepsilon^{\alpha}_{\mathbf{q}}\right) \delta\left(\varepsilon^{\alpha}_{\mathbf{q}} + E_{\mathbf{k}} - E_{\mathbf{k}'}\right), \quad (4)$$

where $n_B(\cdot)$ is a Bose distribution function, T_e is the temperature of the metal, and $n_I(\cdot)$ is the magnon distribution in the insulating layers. At thermal equilibrium, $n_I(\varepsilon) = n_B([\varepsilon - \mu^{\alpha}]/k_B T_{\alpha})$. Accordingly, we obtain an expression for the β magnons. For the case where the ferromagnetically ordered planes of the NiO layer are in parallel to the interface, only one of the sublattices of NiO couples to the metal in our model and the matrix elements $V^{\alpha,\beta}_{\mathbf{q}\mathbf{k}\mathbf{k}'}$ are obtained by using the Bogoliubov transformation to express the lattice magnons describing the local spin excitations at the interface by the magnonic eigenstates,

$$V^{\alpha}_{\mathbf{q}\mathbf{k}\mathbf{k}'} = \sqrt{2s} J_I \frac{\sin(k_x)\sin(k'_x)}{N_x^{\rm NM}} \frac{\eta(\mathbf{q}_{\parallel}) \delta_{\mathbf{k}_{\parallel}+\mathbf{q}_{\parallel},\mathbf{k}'_{\parallel}} u_{\mathbf{q}0}}{\sqrt{N^I}}, \quad (5)$$

where $\eta(\mathbf{q}_{\parallel}) = [e^{-iq_z/\sqrt{6}} + 2e^{iq_z/2\sqrt{6}} \cos(q_y/2\sqrt{2})]$ follows from the lattice structure and $u_{\mathbf{q}0}$ is the amplitude of the magnonic eigenstate with momentum $\mathbf{q}$ at the interface. The terms $\sin(k_x)$ and $\sin(k'_x)$ are the amplitude of the electronic solutions of the tight-binding Hamiltonian at the interface. With this, we can write the equation for the α current slightly more conveniently as

$$I^{\alpha} = \frac{s\pi J_I^2}{\hbar} \sum_{\Delta k_y \Delta k_z} \left\{ |\eta(\Delta\mathbf{k}_{\parallel})|^2 \left[\sum_{k_y k_z} \frac{\sin^2(k_x)}{\partial E_{\mathbf{k}}/\partial k_x} \frac{\sin^2(k'_x)}{\partial E_{\mathbf{k}'}/\partial k'_x} \right] \times \sum_{q_x} |u_{\Delta\mathbf{k}_{\parallel},q_x,0}|^2 \left[\varepsilon^{\alpha}_{\mathbf{q}} + \Delta\mu\right] \times \left[n_B\left(\frac{\varepsilon^{\alpha}_{\mathbf{q}} + \Delta\mu}{k_B T_e}\right) - n_I\left(\varepsilon^{\alpha}_{\mathbf{q}}\right) \right] \right\}, \quad (6)$$

where there is a dependence on the number of atomic layers of both the AFMI and the FMI only in the second line of Eq. (6). Let us consider the situation $\Delta\mu = 0$. Note that we have the following normalization condition due to the paraunitarity of the Bogoliubov transformation,

$$\sum_{q_x} |u_{\Delta\mathbf{k}_{\parallel},q_x,0}|^2 h(q_x) = (-1)^{N_M}, \quad (7)$$

where $h(q_x) = 1$ for spin-(-1) magnon operators (α) and $h(q_x) = -1$ for spin-1 magnon operators (β) mode, and N_M is the number of atomic NiO planes. Furthermore, we consider now that magnons also to be in quasiequilibrium at temperature T_M, $n_I(\varepsilon^{\alpha}_{\mathbf{q}}) = n_B(\varepsilon^{\alpha}_{\mathbf{q}}/k_B T_m)$. Now, we can compute the differential spin current (see Fig. 3) and the integrated spin current (see Fig. 4). While $\varepsilon[n_B(\varepsilon/k_B T_e) - n_B(\varepsilon/k_B T_m)]$ is not a constant as a function of ε, it gets smoother with increasing temperature due to the properties of the Bose-Einstein distribution. Consequently, the magnon spin transport at higher temperatures is mainly determined by the normalization condition Eq. (7). Figure 4 shows the amplitude of the spin current that increases with increasing temperature due to a larger number of thermally excited magnons at higher temperature. Furthermore, we see that the differences in spin current for

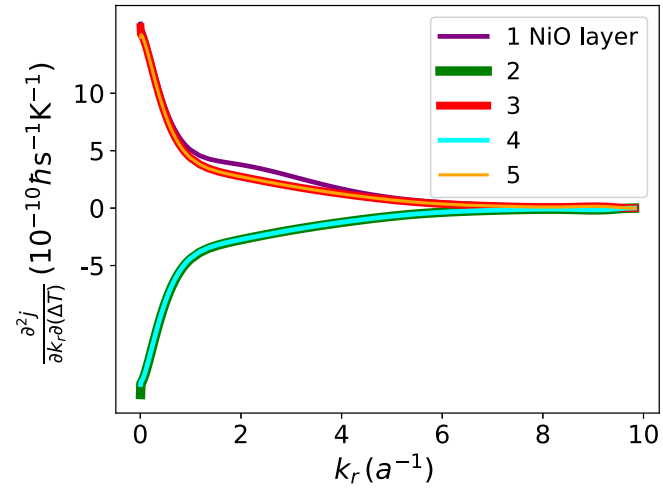

FIG. 3. Differential spin current density per thermal gradient, $\partial^2 j/[\partial k_r \partial(\Delta T)]$, as a function of the in-plane absolute momentum transfer $k_r = \sqrt{(\Delta k_y)^2 + (\Delta k_z)^2}$ at $T = 300$ K for different numbers of atomic layers of NiO. The number of ferromagnetic layers is always five. Note the qualitative difference between even and odd.

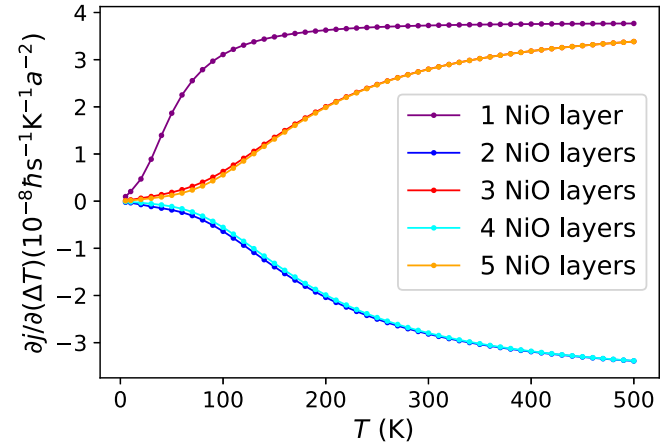

FIG. 4. Spin current density per thermal gradient, i.e., the spin Seebeck coefficient, for an exchange coupling to the metal of $J_I = 1$ K, where a is the lattice constant of NiO. We see that for increasing temperatures, the only remaining thickness dependence is the even-odd effect, i.e., the sign of the spin current density depending on the number of NiO atomic planes being even or odd.

NiO layers of the same parity tends to vanish with increasing temperature. This is due to Eq. (6) being increasingly dominated by the influence of the amplitudes $u_{\Delta\mathbf{k}_\parallel,q_x,0}$ and those are subject to a normalization criterion as discussed above.

V. DISCUSSION AND SUMMARY

In this paper, we considered perfect crystals of NiO which has higher Néel temperatures than polycrystalline NiO as experimentally investigated in Refs. [1,3]. Furthermore, the exchange coupling between the insulators in our model is strong which should result in a high blocking temperature so that the order of the NiO layer should be pinned by the magnetization of the FMI. This is consistent with the result that the amplitude of the spin current is monotonously increasing with increasing temperature such as in the experiments by Baldrati *et al.* [14] in contrast to the peak in the temperature dependence found by Ref. [3] for polycrystalline NiO. Our theoretical results heavily depend on the crystalline orientation in the (111) direction. For other orientations, we expect a different behavior as the interface will most likely be compensated, e.g., for NiO in the (100) direction. Note that a dependence on the crystalline order was experimentally found for Cr_2O_3 layers [22]. Further note that a spin-transfer torque between two ferromagnets based on thermally driven spin current through an antiferromagnet with compensated surfaces was theoretically investigated in Ref. [23].

To provide a more intuitive and less technical description of the even-odd effect, we point out that the sign of the spin current is determined by the magnetic orientation of the insulating layer next to the metal. This is due to the fact that for a layer magnetized in the $+z$ direction, i.e., it belongs to the A sublattice, the magnons in the $-z$ direction have a higher amplitude on this layer than $+z$ magnons, and the other way around for a layer belonging to the B sublattice. The amplitude on the interfacing layer is crucial for the spin current. The magnetization of the layer next to the metal is—in return—determined by the number of NiO layers being even or odd as the magnetization of the layer next to the ferromagnetic insulator is pinned.

Although the focus of this work was the antiferromagnet NiO, the results, especially the predicted even-odd effect, are relevant for other materials. Namely, enhanced spin transport was already measured for CoO instead of NiO in Ref. [3]. The requirement for a precisely defined number of layers could also be achieved in magnetic van der Waals materials [24]. Here, specifically a layered antiferromagnet such as CrI_3 [25] is of interest.

We have computed the spin current between a ferromagnetic insulator and a heavy metal through a thin NiO layer in the clean limit and found a strong even-odd effect for the spin current. Moreover, at higher temperature, the influence of the NiO layer thickness apart from the even-odd effect vanishes. It remains an open question how details of a real system including damping will influence the spin current. However, our results suggest that as long as the magnetic structure in NiO is pinned by the FMI, the even-odd effect could be observed in experiment with the remaining challenge that a sample needs to be prepared with a precise number of atomic planes.

ACKNOWLEDGMENTS

We thank Ran Cheng for useful comments. This work was supported by the German Research Foundation (DFG) via Project No. 417034116 and by the Research Council of Norway through its Centres of Excellence funding scheme, Project No. 262633, "QuSpin."

APPENDIX: MAGNONIC EIGENSTATES

In this Appendix, we show the details of the calculations of magnonic eigenstates.

1. Holstein-Primakoff transformation

We use a standard Holstein-Primakoff transformation to express the spin operators on the lattice sites by bosonic operators $a_{\mathbf{r}}^{(\dagger)}$ for lattice sites $\mathbf{r}$ where in the presumed ground state the spins point in the z direction, i.e., on the A sublattice and $b_{\mathbf{r}}^{(\dagger)}$ where it points in the $-z$ direction (B planes). The Holstein-Primakoff transformation reads (we truncate after second order in the bosonic operators)

$$S_r^z = \hbar(s - a_{\mathbf{r}}^\dagger a_{\mathbf{r}}), \quad S_{\mathbf{r}}^+ = \hbar\sqrt{2}a_{\mathbf{r}}, \quad S^-\mathbf{r} = \hbar\sqrt{2s}a_{\mathbf{r}}^\dagger \tag{A1}$$

for the A sublattice and

$$S_r^z = \hbar(-s + b_{\mathbf{r}}^\dagger b_{\mathbf{r}}), \quad S_{\mathbf{r}}^+ = \hbar\sqrt{2}b_{\mathbf{r}}^\dagger, \quad S^-\mathbf{r} = \hbar\sqrt{2s}b_{\mathbf{r}} \tag{A2}$$

for the B sublattice, $S_{\mathbf{r}}^x = (S_{\mathbf{r}}^+ + S_{\mathbf{r}}^-)/2$, $S_{\mathbf{r}}^y = (S_{\mathbf{r}}^+ - S_{\mathbf{r}}^-)/(2i)$.

2. In-plane Fourier transform

We perform a Fourier transform in the yz plane and call the resulting operators $a_{j,\mathbf{q}_\parallel}^{(\dagger)}$ and $b_{j,\mathbf{q}_\parallel}^{(\dagger)}$, where $\mathbf{q}_\parallel$ is the in-plane momentum and j the index of the plane in x direction.

3. Magnonic eigenstates of AFMI-FMI system

We present here the formalism of the two-flavor Bogoliubov transformation for the case of M atomic NiO layers and N atomic FMI layers. After the in-plane Fourier transform, the Hamiltonian can be denoted as

$$H = \sum_{\mathbf{q}_\parallel} (\Psi_{\mathbf{k}_\parallel}^\dagger, \Psi_{-\mathbf{k}_\parallel}) \mathcal{H}_{\mathbf{k}_\parallel} \begin{pmatrix} \Psi_{\mathbf{k}_\parallel} \\ \Psi_{-\mathbf{k}_\parallel}^\dagger \end{pmatrix}, \tag{A3}$$

where $\Psi_{\mathbf{q}_\parallel} = (b_{1,-\mathbf{q}_\parallel}^\dagger, a_{2,\mathbf{q}_\parallel}, \ldots, b_{M,-\mathbf{q}_\parallel}^\dagger, a_{M+1,\mathbf{q}_\parallel}, a_{M+2,\mathbf{q}_\parallel}, \ldots, a_{N+M,\mathbf{q}_\parallel})^T$ for an odd M and $\Psi_{\mathbf{q}_\parallel} = (a_{1,\mathbf{k}_\parallel}, b_{2,-\mathbf{k}_\parallel}^\dagger, \ldots, b_{M,-\mathbf{k}_\parallel}^\dagger, a_{M+1,\mathbf{k}_\parallel}, a_{M+2,\mathbf{k}_\parallel}, \ldots, a_{N+M,\mathbf{k}_\parallel})^T$ for even M. The matrix Hamiltonian is thus

$$\mathcal{H}_{\mathbf{k}_\parallel} = \begin{pmatrix} \mathcal{A}_{\mathbf{q}_\parallel} & \mathcal{B} \\ \mathcal{B} & \mathcal{A}_{\mathbf{q}_\parallel} \end{pmatrix}, \tag{A4}$$

where the matrix elements

$$\mathcal{A}_{\mathbf{k}_\parallel} = \begin{pmatrix} d_1 & c_a & & & & & & & & \\ c_a^* & d_a & \ddots & & & & & & & \\ & \ddots & \ddots & \ddots & & & & & & \\ & & c_a^* & d_a & c_a & & & & & \\ & & & c_a^* & d_M & c_{af} & & & & \\ & & & & c_{af}^* & d_{M+1} & c & & & \\ & & & & & c^* & d & c & & \\ & & & & & & c^* & d & \ddots & \\ & & & & & & & \ddots & \ddots & \ddots \\ & & & & & & & & c^* & d & c \\ & & & & & & & & & c^* & d_{N+M} \end{pmatrix} \tag{A5}$$

and

$$\mathcal{B} = \frac{S(D_1 - D_2)}{2} \begin{pmatrix} 1_{M\times M} & 0_{M\times N} \\ 0_{N\times M} & 0_{N\times N} \end{pmatrix}, \tag{A6}$$

where $1_{M\times M}$ is the $M \times M$ identity matrix and $0_{i\times j}$ is an $i \times j$ matrix with zeros only. The coefficients in $\mathcal{A}_{\mathbf{k}_\parallel}$ are

$$\begin{aligned} d_1 &= S\big(J_1\gamma_{\mathbf{q}_\parallel}^{(1)} + 3J_2 - 3J_1\big), \\ d_a &= S\big(J_1\gamma_{\mathbf{q}_\parallel}^{(1)} + 6J_2\big), \\ c_a &= S\big(J_1\gamma_{\mathbf{q}_\parallel}^{(2)} + J_2\gamma_{\mathbf{q}_\parallel}^{(3)}\big), \\ d_M &= S\big(J_1\gamma_{\mathbf{q}_\parallel}^{(1)} + 3J_2 - 3J_1\big) + 3S_F(J_{I1} + J_{I2}), \\ c_{af} &= \sqrt{S_F S}\big(J_{I1}\gamma_{\mathbf{q}_\parallel}^{(2)} + J_{I2}\gamma_{\mathbf{q}_\parallel}^{(3)}\big), \\ d_{M+1} &= S_F J_F\big(\gamma_{\mathbf{q}_\parallel}^{(1)} - 9\big) + 3S(J_{I1} + J_{I2}), \\ d &= S_F J_F\big(\gamma_{\mathbf{q}_\parallel}^{(1)} - 12\big) + 2S_F K_F, \\ c &= S_F J_F \gamma_{\mathbf{q}_\parallel}^{(2)}, \\ d_{M+N} &= S_F J_F\big(\gamma_{\mathbf{q}_\parallel}^{(1)} - 9\big) + 2S_F K_F, \end{aligned} \tag{A7}$$

and

$$\gamma_{\mathbf{k}_\parallel}^{(1)} = 2\left[2\cos\left(\frac{k_y}{2\sqrt{2}}\right)\cos\left(\frac{\sqrt{3}k_z}{2\sqrt{2}}\right) + \cos\left(\frac{k_y}{\sqrt{2}}\right)\right], \tag{A8}$$

$$\gamma_{\mathbf{k}_\parallel}^{(2)} = e^{ik_z/\sqrt{6}} + 2e^{-ik_z/(2\sqrt{6})}\cos\left(\frac{k_y}{2\sqrt{2}}\right), \tag{A9}$$

$$\gamma_{\mathbf{k}_\parallel}^{(3)} = \gamma_{-2\mathbf{q}_\parallel}^{(2)}. \tag{A10}$$

Later, we determine the dynamical matrix by multiplying $\mathcal{H}_{\mathbf{q}_\parallel}$ with $\mathcal{G}$ where

$$\mathcal{G}_{ij} = [\psi_{i,\mathbf{q}_\parallel}, \psi_{j,\mathbf{q}_\parallel}^\dagger], \tag{A11}$$

where $\psi_{i,\mathbf{q}_\parallel}^\dagger$ and $\psi_{j,\mathbf{q}_\parallel}^\dagger$ are the elements of $[\Psi_{\mathbf{q}_\parallel}, (\Psi_{\mathbf{q}_\parallel})^\dagger]$ and $[(\Psi_{\mathbf{q}_\parallel})^\dagger, \Psi_{-\mathbf{k}_\parallel}]$, respectively. We diagonalize the matrices $\mathcal{G}\mathcal{H}_{\mathbf{q}_\parallel}$, i.e., we obtain the eigenenergies and amplitudes of the magnonic eigenstates on the lattice sites by solving the eigenvalue problem [15]

$$\mathcal{G}\mathcal{H}_{\mathbf{q}_\parallel}\mathbf{u}_{\mathbf{q}_\parallel} = \pm\varepsilon_{\mathbf{q}_\parallel}\mathbf{u}_{\mathbf{q}_\parallel}, \tag{A12}$$

where $\varepsilon_{\mathbf{q}_\parallel}$ has to be one of the eigenenergies (for in-plane magnon momentum $\mathbf{q}_\parallel$) and $\mathbf{u}_{\mathbf{q}_\parallel}$ is a vector of the amplitudes on each layer of the magnonic eigenstate. The $\pm$ symbol is necessary due to the pseudounitary behavior of the Bogoliubov transformation (while the magnon energies are all positive). For the different solutions we formally assign an index q_x. The creation and annihilation operators of the magnonic eigenstates will be denoted $\alpha^{(\dagger)}$ if they have more weight on the A layers and $\beta^{(\dagger)}$ if they have more weight on the B layers). We need the amplitude on the layer facing the metal, $u_{\mathbf{q}_\parallel,q_x,0}$, for the calculation of the spin current through the metal-insulator interface. We solve Eq. (A12) numerically for convenience.

4. Correction to the spin of the α and β magnons due to NiO anisotropies

If the anisotropies D_1 and D_2 were zero, the matrix elements of $\mathcal{B}$ would vanish. Then the α magnons would carry spin of $-\hbar$ in the z direction and the β magnons would carry a spin of $+\hbar$ in the z direction. The finite matrix elements in $\mathcal{B}$ yield a correction to the spin of the α and β magnons [26]. In the main text, we set $D_1 = D_2 = 0$, ignoring this spin correction (along with the influence of D_1 and D_2 on the magnon spectrum) in order to obtain a more intuitive understanding of the even-odd effect (also see the following section of this Appendix). If we take finite D_1 and D_2 into account in our numerical calculations, we find an additional contribution to the spin current (see Fig. 5). We see that this contribution is more significant relative to the absolute value of the current for smaller temperatures.

5. Normalization condition

In the general case, including finite anisotropies D_1 and D_2 [see Eq. (1)], each eigenstate of the dynamical matrix is a superposition of $a_{j,\mathbf{q}_\parallel}$, $a_{j,-\mathbf{q}_\parallel}^\dagger$ (j as the index of A planes), $b_{j,\mathbf{q}_\parallel}$, and $b_{j,-\mathbf{q}_\parallel}^\dagger$ (j as the index of B planes). However, the mixing of $a_{j,\mathbf{q}_\parallel}$ with $a_{j,-\mathbf{q}_\parallel}^\dagger$ as well as $b_{j,\mathbf{q}_\parallel}$ with $b_{j,-\mathbf{q}_\parallel}^\dagger$ turns out to be a

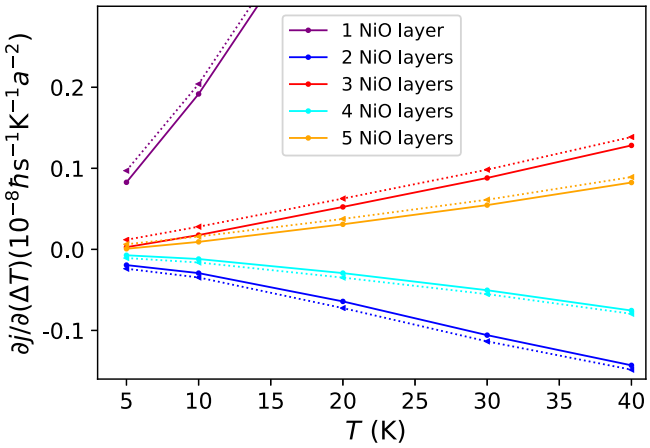

FIG. 5. The spin current through the metal-insulator interface as a function of temperature: for vanishing anisotropies ($D_1 = D_2 = 0$) (circles connected by solid lines) and for finite anisotropies ($D_1 = 1.13$ K, and $D_2 = 0.06$ K) (triangles connected by dotted lines). We plot here the smaller temperatures for better visibility. The relative correction due to finite D_1 and D_2 gets smaller and smaller with increasing temperature.

small effect and is negligible at least for higher temperatures, due to the small values of D_1 and D_2. So, in order to obtain an intuitive understanding of the even-odd effect, we can set them to zero. Then only $a_{j,\mathbf{q}_\parallel}$ and $b^\dagger_{j,-\mathbf{q}_\parallel}$ are mixed (α or $\beta^\dagger$) or $b_{j,\mathbf{q}_\parallel}$ and $a^\dagger_{j,-\mathbf{q}_\parallel}$ (β or $\alpha^\dagger$). Then for each magnon, identified by q_x, the normalization condition (following from the Bogoliubov transformation) reads

$$\sum_j g(q_x, j)|u_{\Delta\mathbf{q}_\parallel,q_x,j}|^2 = h(q_x), \tag{A13}$$

where j is now just the plane index in real space, $g(q_x, j) = 1$ for α magnons (spin -1) on A layers and β magnons on B layers, whereas $g(q_x, j) = -1$ for α magnons on B layers and β magnons on A layers. This normalization condition guarantees the correct bosonic commutation relations for the magnons. If we sort the $\alpha^{(\dagger)}$ and $\beta^{(\dagger)}$ analogously to the $a^{(\dagger)}$ and the $b^{(\dagger)}$ operators being sorted in $(\Psi^T_{\mathbf{k}_\parallel})^\dagger$ and $\Psi_{-\mathbf{k}_\parallel}$, we can write the transformation matrix U with $\mathbf{u}_{\mathbf{q}_\parallel,q_x}$ as columns of U. Then the normalization condition is $U^\dagger \mathcal{G} U = \mathcal{G}$. We find easily that we have a similar normalization condition when summing over the magnon amplitudes at one layer,

$$\sum_{q_x} g(q_x, 0)|u_{\Delta\mathbf{q}_\parallel,q_x,0}|^2 = (-1)^{N_M}, \tag{A14}$$

where we have a plus on the right-hand side if layer 0 (the one facing the metal) is an A layer and minus if it is a B layer.

[1] H. Wang, C. Du, P. C. Hammel, and F. Yang, Antiferromagnonic spin transport from $Y_3Fe_5O_{12}$ into NiO, Phys. Rev. Lett. **113**, 097202 (2014).

[2] H. Wang, C. Du, P. C. Hammel, and F. Yang, Spin transport in antiferromagnetic insulators mediated by magnetic correlations, Phys. Rev. B **91**, 220410(R) (2015).

[3] W. Lin, K. Chen, S. Zhang, and C. L. Chien, Enhancement of thermally injected spin current through an antiferromagnetic insulator, Phys. Rev. Lett. **116**, 186601 (2016).

[4] S. M. Rezende, R. L. Rodríguez-Suárez, and A. Azevedo, Diffusive magnonic spin transport in antiferromagnetic insulators, Phys. Rev. B **93**, 054412 (2016).

[5] R. Khymyn, I. Lisenkov, V. S. Tiberkevich, A. N. Slavin, and B. A. Ivanov, Transformation of spin current by antiferromagnetic insulators, Phys. Rev. B **93**, 224421 (2016).

[6] T. Shang, Q. F. Zhan, H. L. Yang, Z. H. Zuo, Y. L. Xie, L. P. Liu, S. L. Zhang, Y. Zhang, H. H. Li, B. M. Wang, Y. H. Wu, S. Zhang, and R.-W. Li, Effect of NiO inserted layer on spin-Hall magnetoresistance in Pt/NiO/YIG heterostructures, Appl. Phys. Lett. **109**, 032410 (2016).

[7] B.-W. Dong, L. Baldrati, C. Schneider, T. Niizeki, R. Ramos, A. Ross, J. Cramer, E. Saitoh, and M. Kläui, Antiferromagnetic NiO thickness dependent sign of the spin Hall magnetoresistance in γ-Fe_2O_3/NiO/Pt epitaxial stacks, Appl. Phys. Lett. **114**, 102405 (2019).

[8] D. Zhu, T. Zhang, X. Fu, R. Hao, A. Hamzić, H. Yang, X. Zhang, H. Zhang, A. Du, D. Xiong, K. Shi, S. Yan, S. Zhang, A. Fert, and W. Zhao, Sign change of spin-orbit torque in Pt/NiO/CoFeB structures, Phys. Rev. Lett. **128**, 217702 (2022).

[9] L. Zhu, L. Zhu, and R. A. Buhrman, Fully spin-transparent magnetic interfaces enabled by the insertion of a thin paramagnetic NiO layer, Phys. Rev. Lett. **126**, 107204 (2021)

[10] M. Dąbrowski, T. Nakano, D. M. Burn, A. Frisk, D. G. Newman, C. Klewe, Q. Li, M. Yang, P. Shafer, E. Arenholz, T. Hesjedal, G. van der Laan, Z. Q. Qiu, and R. J. Hicken, Coherent transfer of spin angular momentum by evanescent spin waves within antiferromagnetic NiO, Phys. Rev. Lett. **124**, 217201 (2020).

[11] G. R. Hoogeboom, G.-J. N. Sint Nicolaas, A. Alexander, O. Kuschel, J. Wollschläger, I. Ennen, B. J. van Wees, and T. Kuschel, Role of NiO in the nonlocal spin transport through thin NiO films on $Y_3Fe_5O_{12}$, Phys. Rev. B **103**, 144406 (2021).

[12] A. Prakash, J. Brangham, F. Yang, and J. P. Heremans, Spin Seebeck effect through antiferromagnetic NiO, Phys. Rev. B **94**, 014427 (2016).

[13] J. Cramer, U. Ritzmann, B.-W. Dong, S. Jaiswal, Z. Qiu, E. Saitoh, U. Nowak, and M. Kläui, Spin transport across antiferromagnets induced by the spin Seebeck effect, J. Phys. D: Appl. Phys. **51**, 144004 (2018).

[14] L. Baldrati, C. Schneider, T. Niizeki, R. Ramos, J. Cramer, A. Ross, E. Saitoh, and M. Kläui, Spin transport in multilayer systems with fully epitaxial NiO thin films, Phys. Rev. B **98**, 014409 (2018).

[15] H. T. Simensen, R. E. Troncoso, A. Kamra, and A. Brataas, Magnon-polarons in cubic collinear antiferromagnets, Phys. Rev. B **99**, 064421 (2019).

[16] M. T. Hutchings and E. J. Samuelsen, Measurement of spin-wave dispersion in NiO by inelastic neutron scattering and its relation to magnetic properties, Phys. Rev. B **6**, 3447 (1972).

[17] T. Holstein and H. Primakoff, Field dependence of the intrinsic domain magnetization of a ferromagnet, Phys. Rev. **58**, 1098 (1940).

[18] R. L. Smit, S. Keupert, O. Tsyplyatyev, P. A. Maksimov, A. L. Chernyshev, and P. Kopietz, Magnon damping in the zigzag phase of the Kitaev-Heisenberg-Γ model on a honeycomb lattice, Phys. Rev. B **101**, 054424 (2020).

[19] H. Adachi, K.-I. Uchida, E. Saitoh, and S. Maekawa, Theory of the spin Seebeck effect, Rep. Prog. Phys. **76**, 036501 (2013).

[20] S. A. Bender, R. A. Duine, and Ya. Tserkovnyak, Electronic pumping of quasiequilibrium Bose-Einstein-condensed magnons, Phys. Rev. Lett. **108**, 246601 (2012).

[21] E. L. Fjærbu, N. Rohling, and A. Brataas, Electrically driven Bose-Einstein condensation of magnons in antiferromagnets, Phys. Rev. B **95**, 144408 (2017).

[22] J. Qin, D. Hou, C. Chen, E. Saitoh, and X. Jin, Crystalline dependence of spin transmission in Cr_2O_3 thin films, J. Magn. Magn. Mater. **501**, 166362 (2020)

[23] R. Cheng, D. Xiao, and J.-G. Zhu, Antiferromagnet-based magnonic spin-transfer torque, Phys. Rev. B **98**, 020408(R) (2018).

[24] J. F. Sierra, J. Fabian, R. K. Kawakami, S. Roche, and S. O. Valenzuela, Van der Waals heterostructures for spintronics and opto-spintronics, Nat. Nanotechnol. **16**, 856 (2021).

[25] B. Huang, G. Clark, E. Navarro-Moratalla, D. R. Klein, R. Cheng, K. L. Seyler, D. Zhong, E. Schmidgall, M. A. McGuire, D. H. Cobden, W. Yao, D. Xiao, P. Jarillo-Herrero, and X. Xu, Layer-dependent ferromagnetism in a van der Waals crystal down to the monolayer limit, Nature (London) **546**, 270 (2017).

[26] A. Kamra, U. Agrawal, and W. Belzig, Noninteger-spin magnonic excitations in untextured magnets, Phys. Rev. B **96**, 020411(R) (2017).